ACS Energy LETTERS

http://pubs.acs.org/journal/aelccp

Metal Monolayers on Command: Underpotential Deposition at Nanocrystal Surfaces: A Quantitative *Operando* Electrochemical Transmission Electron Microscopy Study

Yao Yang, Yu-Tsun Shao, Francis J. DiSalvo, David A. Muller,* and Héctor D. Abruña*

Cite This: *ACS Energy Lett.* 2022, 7, 1292−1297

Read Online

ACCESS | Metrics & More | Article Recommendations | Supporting Information

ABSTRACT: **Underpotential deposition (UPD) enables the generation of metal monolayers whose electronic properties can be significantly different from the bulk. While studied extensively for bulk electrodes, UPD kinetics for individual nanoparticles can deviate from their bulk counterparts due to the distinct differences in the distribution of local electric fields. UPD's nature remains largely unexplored due to the lack of nanoscale time-resolved *operando*/*in situ* techniques at interfaces. This study presents an investigation on a model system, the UPD of monolayer Cu at single-crystal Au nanocube surfaces, based on a correlative analysis of electrochemical results and high-resolution chemical mapping. *Operando* electrochemical liquid-cell scanning transmission electron microscopy (EC-STEM) directly visualizes the potential-dependent and spatially resolved Cu electrodeposition kinetics, classified as planar, island-shaped, or dendritic growth. *Operando* EC-STEM reveals the well-defined diffusion-controlled processes during Cu electrodeposition in sub-μm thick liquid with both quantitative electrochemistry and quantitative imaging analysis. 4D-STEM shows that the Cu electrodeposition is guided by the crystallographic orientation of the Au substrate. This methodology of *operando* EC-STEM for quantitative electrochemistry can serve as a generalized platform to advance fundamental understanding of (electro)chemical reaction dynamics.**

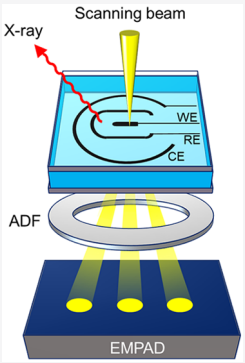

Metal deposition on solid surfaces is important for both fundamental surface science and technological applications, such as metal coating, corrosion prevention, and electrocatalysts.[1,2] Cu electrodeposition has been employed as a model system for understanding nucleation and growth mechanisms and is widely used for fabricating electrical interconnects in integrated circuits.[3] Of particular note is the underpotential deposition (UPD), in which a metal monolayer is electrodeposited on a foreign metal substrate at significantly less negative potentials than that for electrodeposition on the same metal.[4] Cu UPD on bulk electrodes, especially Au and Pt single crystals, has been extensively investigated by pure electrochemical methods,[5−7] *operando*/*in situ* X-ray methods,[8−12] and scanning probe microscopies.[13−16] Early studies by Ross et al. used liquid-cell TEM imaging to investigate bulk Cu electrodeposition on polycrystalline Au and Pt electrodes.[17,18] Recently, Cu UPD on nanocrystal surfaces, together with galvanic displacement, have been widely used to precisely deposit monolayers of precious metals on less expensive or nonprecious substrates to maximize the utilization of precious metals as electrocatalysts.[19−26] However, Cu UPD processes at practical nanocrystal surfaces remain largely unknown due to the lack of temporarily resolved *operando*/*in situ* techniques at the nm scale.[27] With small, finite sizes, nanocrystals can (and often do) have different/distinct local electric field distributions at terraces, steps, edges, and kinks and can exhibit an increased (and dramatically different) field concentration and reactivity relative to their bulk counterparts. The local electric field largely determines the driving force and concentration gradients of solution species at and near the surface and, thus, has a significant impact on charge transfer kinetics and overall (electro)catalytic reaction mechanisms. Here, we employ *operando* EC-STEM to track

Received: January 26, 2022
Accepted: March 7, 2022
Published: March 9, 2022

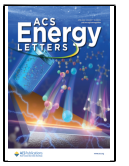

https://doi.org/10.1021/acsenergylett.2c00209
ACS Energy Lett. 2022, 7, 1292−1297

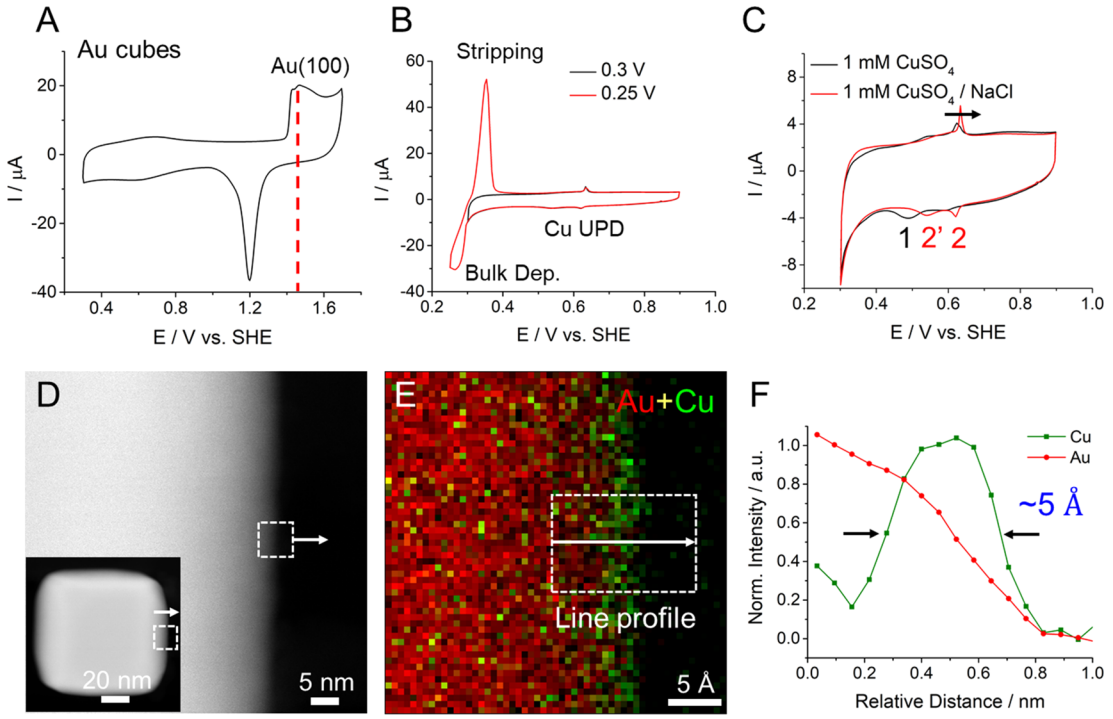

Figure 1. Cu electrodeposition in a standard three-electrode cell. (A) CV profile of Au nanocubes in Ar-sat. 0.1 M H_2SO_4 at 100 mV/s. (B) CV profiles of Cu UPD and bulk deposition in Ar-sat. 1 mM $CuSO_4$/0.1 M H_2SO_4 at 5 mV/s. (C) CV profiles of Cu UPD in Ar-sat. 1 mM $CuSO_4$/0.1 M H_2SO_4 with/without 1 mM NaCl. (d–f) HAADF-STEM images of an Au nanocube after Cu UPD and EELS composite maps of Au (red) and Cu (green) and line profiles. It should be noted that the measured 5 Å width represents an upper limit to the actual thickness of the Cu monolayer due to sample mistilts and beam spreading, as the sample is ~10× as thick as the depth of field.

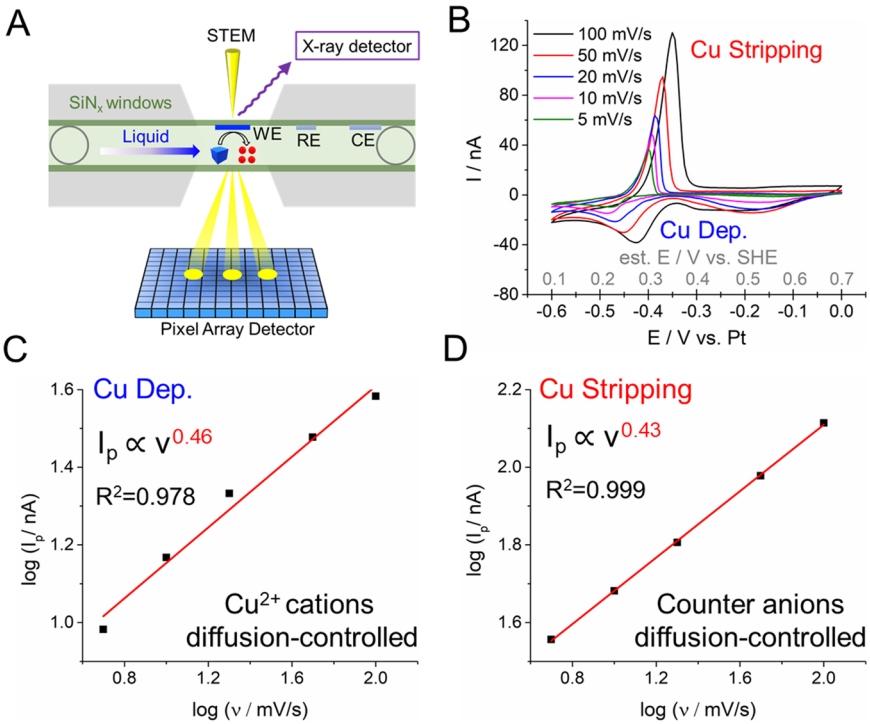

Figure 2. (A) Schematic of *operando* EC-STEM cell with the capability to enable reliable electrochemistry and simultaneously track dynamic evolution under operating conditions. (B) CV profiles of Cu electrodeposition on Au nanocubes in Ar-sat. 1 mM $CuSO_4$/0.1 M $NaClO_4$ in the EC-STEM. (C,D) Quantitative analysis of peak currents in (b) vs scan rate, showing that both Cu deposition and stripping processes are diffusion-controlled.

the dynamic morphological and structural evolution during Cu electrodeposition on single-crystal Au nanocubes.

Au nanocubes (~100 nm) were selected as well-defined nanocrystal surfaces for Cu UPD. Cyclic voltammetry (CV)

https://doi.org/10.1021/acsenergylett.2c00209
ACS Energy Lett. 2022, 7, 1292−1297

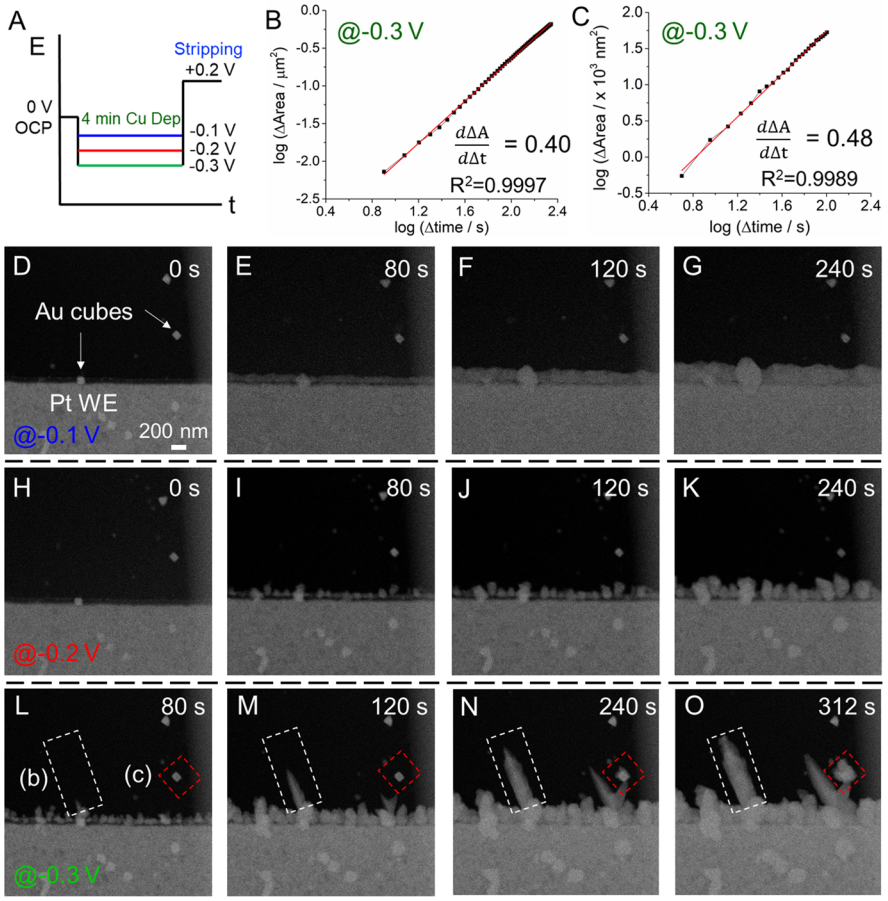

Figure 3. *Operando* EC-STEM during Cu electrodeposition under steady-state conditions. (A) Experimental procedures of Cu electrodeposition at −0.1, −0.2, and −0.3 V followed by stripping at +0.2 V vs Pt. (B,C) Quantitative STEM imaging analysis of the area increase vs time of two Cu particles in the white and red boxes labeled (b) and (c), respectively, in Figure 3L. (D−O) *Operando* EC-STEM movies of Cu electrodeposition at −0.1, −0.2, and −0.3 V, respectively, at the identical location.

profiles of Au nanocubes in a standard three-electrode electrochemical cell exhibit the characteristic oxidation peak of Au(100) facets at ∼1.45 V vs SHE (Figure 1A), which matches well with that of Au(100) single crystals at ∼1.45 V vs SHE (Figure S1).[28] The CV profiles in 1 mM $CuSO_4$, with different lower potential limits, exhibit the characteristic Cu UPD peak followed by bulk Cu deposition at E < 0.25 V vs RHE and the corresponding sharp Cu stripping peaks (Figure 1B). To further examine whether Cu successfully electrodeposits at Au nanocube surfaces, chloride was selected as an ionic probe to "amplify" the Cu UPD and stripping features (Figure 1C). The addition of 1 mM NaCl in 1 mM $CuSO_4$ converted the broad Cu^{2+}/Cu UPD peak at 0.49 V (peak 1) to sharper Cu^{2+}/CuCl and CuCl/Cu peaks at 0.63 and 0.54 V (peaks 2 and 2′), respectively. The formation of a Cu−Cl adlayer on Au nanocubes at 0.63 V matches results on Au(100) single crystals at 0.63 V in the presence of chloride (Figure S2).[13]

The microstructure of the Cu UPD on Au nanocubes was then examined using an aberration-corrected high-angle annular dark-field (HAADF) STEM equipped with an electron energy loss spectrometer (EELS). HAADF-STEM images in Figure 1D exhibit the well-defined cubic morphology of Au nanocrystals. EELS elemental maps and line profiles revealed the electrodeposited Cu to be around 5 Å thick after Cu UPD at 0.25 V vs SHE for 30 min (Figures 1E,F and S3). The measured 5 Å width is an upper limit to the actual thickness of the Cu monolayer due to sample mistilts and beam spreading, as the sample thickness is ∼10× the depth of field. Bulk Cu electrodeposition onsets at around 0.3 V (Figure 1B). The corresponding STEM-EELS in Figure S4 indicated the formation of a thicker electrodeposited Cu layer (∼3 nm) on Au, followed by the growth of μm-sized Cu clusters. In summary, the correlative analysis of CV profiles and STEM-EELS provides unambiguous evidence of the electrodeposition of monolayer Cu during Cu UPD on {100}-oriented Au surfaces followed by the formation of bulk Cu.

To elucidate the dynamic evolution during Cu electrodeposition at Au nanocubes, we performed *operando* EC-STEM studies. Figure 2A presents a cross section of the *operando* three-electrode EC-STEM cell, including the working, Pt counter, and Pt pseudoreference electrodes (WE, Pt CE, and Pt pseudo-RE) with a liquid thickness of ∼500 nm. In an effort to demonstrate that *operando* EC-STEM can provide reliable electrochemical measurements, we performed Cu electrodeposition on Au nanocubes near the Pt WE at various scan rates in Ar-sat. 1 mM $CuSO_4$/0.1 M $NaClO_4$ (Figure 2B). The Cu UPD peaks in the EC-STEM study are located in the broad peaks at 0.5−0.6 vs SHE, matching the Cu UPD peak position at 0.54 V vs SHE in Figure 1B. CV profiles of Cu electrodeposition exhibit the broad Cu deposition peaks and sharp Cu stripping peaks. The potential of the Pt pseudo-RE (PtO_x/Pt) in this EC-STEM study was estimated to be 0.7−0.8 V vs SHE based on our previous studies (Figure S5).[29,30]

https://doi.org/10.1021/acsenergylett.2c00209
ACS Energy Lett. 2022, 7, 1292−1297

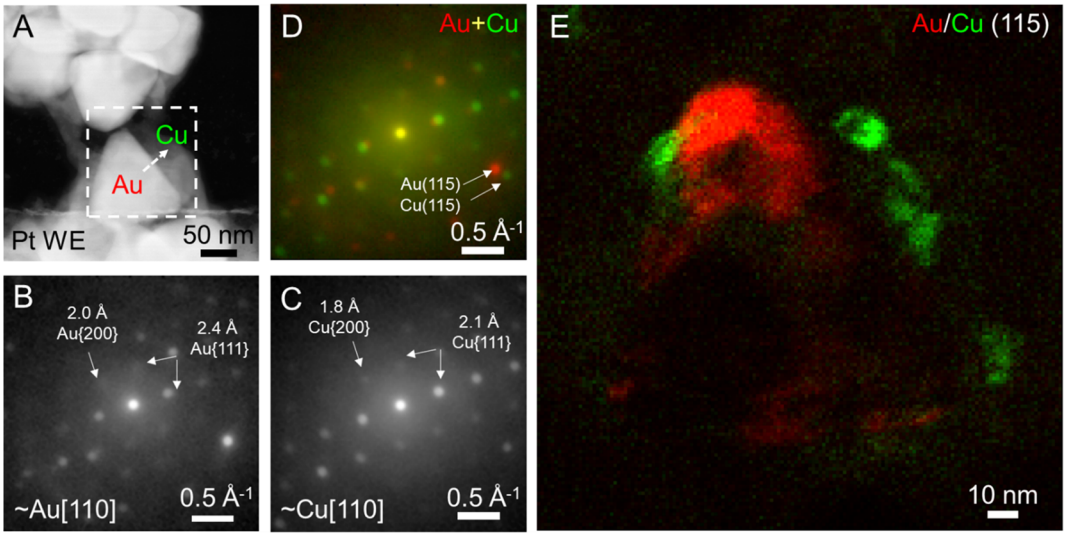

Figure 4. ***Ex situ*** **4D-STEM diffraction imaging of Cu electrodeposited on Au nanocubes from the same setup as previous** ***operando*** **EC-STEM studies. (A) HAADF-STEM image of Cu on Au cubes. (B−D) Diffraction patterns of Au and Cu in the dashed box in (A). (D) Overlay of diffraction patterns for Au (B) and Cu (C). (E) Dark-field 4D-STEM maps of Au (red) and Cu (green) domains extracted from the Cu(115) and Au(115).**

The bulk Cu deposition/stripping peaks are located at around 0.3 V vs SHE, which matches the corresponding peaks obtained from standard electrochemical cells at 0.30 V vs SHE (Figure 2B). Quantitative analysis of the peak currents of Cu electrodeposition results in a correlation of $I_p \propto \nu^{0.46}$, which suggests a diffusion-controlled redox process ($I_p \propto \nu^{0.5}$) (Figure 2C). However, it is intriguing to observe a similar correlation of $I_p \propto \nu^{0.43}$ for the Cu stripping peaks, which is different from results from a conventional electrochemical cell where a surface-controlled stripping process predicts a linear correlation of $I_p \propto \nu$ (Figure 2D). Thus, we propose that the square-root correlation of Cu stripping in EC-STEM is primarily due to the diffusion of anions to counterbalance/compensate the Cu^{2+} generated during Cu stripping. The Randles-Ševčík equation below was used to estimate the diffusion coefficient to be 3.4×10^{-5} cm^2/s based on Cu electrodeposition peaks (details in the SI). It is comparable to the bulk diffusion coefficient of 1 mM $CuSO_4$ (7.4×10^{-6} cm^2/s), given the significant difference between the microelectrode in EC-STEM and bulk electrode in a standard electrochemical cell.[31]

$$I_p = 0.446nFAC\sqrt{\frac{nFD\nu}{RT}}$$

With a rigorous electrochemical protocol established, we performed *operando* EC-STEM of Cu electrodeposition/stripping under steady-state conditions. A reduction potential of −0.1 V, slightly below the open circuit potential (OCP) at 0 V, was able to drive the Cu UPD and bulk Cu electrodeposition at a slow reaction rate (Figure 3A). An oxidation potential of +0.2 V vs Pt was then applied to strip Cu, so the identical region could be used to perform electrodeposition at −0.2 and −0.3 V. *Operando* EC-STEM movies were performed at a very low dose of 2 e^-/nm^2 in a low concentration of Cu^{2+} (1 mM), so that no significant beam-induced Cu deposition artifacts were observed, as evidenced by the identical STEM images before/after the first Cu electrodeposition/stripping measurements (Figure 3D,H). In addition, similar morphologies of electrodeposited Cu were observed in a region under a 4 min beam exposure, relative to a nearby region not under continuous beam exposure, confirming that Cu growth was initiated by the electrochemical reduction rather than beam-induced reduction (Figure S6). At a mild reduction potential of −0.1 V, Cu only electrodeposited noticeably after 80 s (Figures 3D,E and S7 and Movie S1). Cu continued to plate on both Au nanocubes and Pt WE and formed a planar coating of ∼200 nm from 80 to 240 s (Figure 3F−G), which is consistent with the growth by a kinetic roughening process.[18,32] Upon oxidation at +0.2 V, the stripping of the small amount of Cu electrodeposited at −0.1 V was completed within 4 s (Figure S8 and Movie S2). At a medium reduction potential of −0.2 V, Cu electrodeposited within 40 s at an increasing rate, relative to that at −0.1 V. From 40 to 240 s, Cu then continued to grow into 200−500 nm isolated islands (Figures 3H−K and S9 and Movie S3), which shared similar ramified features to early liquid-cell TEM studies.[17] Upon oxidation at +0.2 V, the increasing amount of Cu electrodeposited at −0.2 V began to noticeably strip after 16 s and was completely stripped after 32 s (Figure S10 and Movie S4). Finally, at an aggressive reduction potential of −0.3 V, a significantly larger amount of Cu began to electrodeposit in a dendritic morphology from 80 to 240 s, relative to that formed at −0.2 V. (Figures 3L−O and S11 and Movie S5). In particular, Cu particles (**b**), preferentially grew on the Au nanocubes and formed well-defined μm-sized dendrites (Figure 3M−O). A Cu particle (**c**) initially remained detached from the Pt electrode and thus electrochemically inactive. At 240 s, this particle came into contact with the continuously growing Cu dendrites underneath and was "electrified", which initiated further Cu electrodeposition on this particle from 240 to 312 s (Figures 3N−O and S11). Upon oxidation at +0.2 V, Cu particles (**b**) and (**c**) initially experienced rapid stripping processes within 8−16 s (Figures S12A−C and Movie S6). At 24 s, Cu dendrites underneath the Cu particle (**c**) began to detach and gradually strip, which led to the termination of stripping processes for this particle (Figures S12E−H). Given the large amount of Cu electrodeposited at −0.3 V, residual Cu dendrites were still observed after 96 s (Figures S12I−L).

https://doi.org/10.1021/acsenergylett.2c00209
ACS Energy Lett. 2022, 7, 1292−1297

Cu particles, labeled as (**b**) and (**c**) in Figure 3L, were selected for quantitative analysis of the electrodeposition kinetics after segmenting STEM images from the surrounding liquid background. The growth of particle surface area was plotted as a function of time (Figure 3B,C). Both particles exhibited excellent linear fittings with the first derivative of $\frac{\Delta A}{\Delta t}$ (i.e., the growth rate) with an exponent of ∼0.5, indicating a diffusion-controlled process. Current transients at −0.3 V in EC-STEM meet the criterion of a diffusion-controlled process, based on the Cottrell equation, which matches with the well-defined diffusion-controlled process in a standard electrochemical cell (Figure S13). In addition, the effects of chloride on Cu electrodeposition were also shown as the formation of dendritic Cu with finer branches formed on Au nanocubes (Figures S14 and 15 and Movie S7), which correlates to the pronounced Cu^{2+}/CuCl/Cu redox couples in Figure 1C. We acknowledge that the present *operando* EC-STEM studies primarily focused on tracking the nm-scale electrodeposition of bulk Cu rather than monolayer Cu due to the inherent limitation of spatial resolution in EC-STEM, and a significantly higher beam dose was required for resolving Cu/Au interface at the atomic scale, which may cause undesirable beam-induced damage. Nonetheless, Cu bulk electrodeposition closely follows the monolayer Cu UPD on Au, which, in turn, can provide indirect insights on the Cu UPD mechanisms.

Ex situ 4D-STEM diffraction imaging was performed on the same locations after Cu electrodeposition in EC-STEM studies (Figure 4). 4D-STEM works by using an electron microscope pixel array detector (EMPAD) to record the 2D electron diffraction pattern over a 2D grid of probe positions, which can retrieve spatially resolved structural information at a dramatically reduced beam dose.[33,34] The scanning electron nanobeam diffraction patterns of both the Au nanocube and electrodeposited Cu exhibited the face-centered cubic (fcc) single-crystal features close to the [110] zone axis (Figure 4B,C). The composite image of representative diffraction patterns from Cu and Au clearly demonstrates that Cu electrodeposition was guided by the crystallographic orientation of the Au nanocube substrates (Figure 4D). 4D-STEM dark-field imaging using the two diffraction spots of Au(115) (0.8 Å) and Cu(115) (0.7 Å) (Figures 4D and S16) yielded a false-color map showing crystal domains with crystal orientations matching those two diffraction spots (Figure 4E). The false-color image exhibits ∼10 nm Cu layers on Au nanocubes, which are consistent with our STEM-EELS results under similar electrodeposition conditions (Figure S4). The formation of Cu nanoclusters was further confirmed by additional 4D-STEM analysis and supported by STEM-EDX mapping (Figures S17 and S18). The large 13% lattice mismatch between Au and Cu can rationalize that Cu UPD was followed by the growth of oriented Cu nanoclusters instead of an epitaxial growth, which often requires a <3% lattice mismatch.[35,36]

In summary, *operando* EC-STEM and 4D-STEM have been employed to resolve the potential-dependent kinetics of Cu UPD at nm scale and revealed that the crystal orientation of the diffusion-controlled Cu electrodeposition is guided by the Au nanocube substrates. The strategy of *operando* EC-STEM illustrates the potential to provide a microscopic picture for many electrocatalytic reactions at interfaces, such as fuel cells, water splitting, and CO_2 electroreduction.[37−41]

■ ASSOCIATED CONTENT

Supporting Information

The Supporting Information is available free of charge at https://pubs.acs.org/doi/10.1021/acsenergylett.2c00209.

Experimental Methods and Figures S1−S18 (PDF)

Movies S1−S7 (ZIP)

■ AUTHOR INFORMATION

Corresponding Authors

Héctor D. Abruña − *Department of Chemistry and Chemical Biology, Cornell University, Ithaca, New York 14853, United States;* orcid.org/0000-0002-3948-356X; Email: hda1@cornell.edu

David A. Muller − *School of Applied and Engineering Physics and Kavli Institute at Cornell for Nanoscale Science, Cornell University, Ithaca, New York 14853, United States;* orcid.org/0000-0003-4129-0473; Email: dm24@cornell.edu

Authors

Yao Yang − *Department of Chemistry and Chemical Biology, Cornell University, Ithaca, New York 14853, United States;* Present Address: Miller Institute, Department of Chemistry, UC Berkeley, Berkeley, California 94720, United States. (Y.Y.); orcid.org/0000-0003-0321-3792

Yu-Tsun Shao − *School of Applied and Engineering Physics, Cornell University, Ithaca, New York 14853, United States*

Francis J. DiSalvo − *Department of Chemistry and Chemical Biology, Cornell University, Ithaca, New York 14853, United States*

Complete contact information is available at: https://pubs.acs.org/10.1021/acsenergylett.2c00209

Notes

The authors declare no competing financial interest.

■ ACKNOWLEDGMENTS

This work was primarily supported by the Center for Alkaline-Based Energy Solutions (CABES), part of the Energy Frontier Research Center (EFRC) program supported by the U.S. Department of Energy, under grant DE-SC-0019445. This work made use of TEM facilities at the Cornell Center for Materials Research (CCMR), which are supported through the National Science Foundation Materials Research Science and Engineering Center (NSF MRSEC) program (DMR-1719875). We are grateful to Malcolm (Mick) Thomas at CCMR for the help in Nion UltraSTEM.

■ REFERENCES

(1) Somorjai, G. A. *Chemistry in Two Dimensions: Surfaces*; Cornell University Press, 1981.

(2) Bénard, J., Ed. *Adsorption on Metal Surfaces*; Elsevier: Amsterdam, 1983.

(3) Rosenberg, R.; Edelstein, D. C.; Hu, C.-K.; Rodbell, K. P. Copper Metallization for High Performance Silicon Technology. *Annu. Rev. Mater. Sci.* **2000**, *30*, 229−262.

(4) Herrero, E.; Buller, L. J.; Abruña, H. D. Underpotential Deposition at Single Crystal Surfaces of Au, Pt, Ag and Other Materials. *Chem. Rev.* **2001**, *101*, 1897−1930.

(5) Holzle, M. H.; Zwing, V.; Kolb, D. M. The Influence of Steps on the Deposition of Cu onto Au(111). *Electrochim. Acta* **1995**, *40*, 1237−1247.

(6) Shi, Z.; Wu, S.; Lipkowski, J. Coadsorption of Metal Atoms and Anions: Cu upd in the Presence of SO_4^{2-}, Cl^- and Br^-. *Electrochim. Acta* **1995**, *40*, 9−15.
(7) Omar, I. H.; Pauling, H. J.; Juttner, K. Underpotential Deposition of Copper on Au(III) Single-Crystal Surfaces: A Voltammetric and Rotating Ring Disk Electrode Study. *J. Electrochem. Soc.* **1993**, *140*, 2187−2192.
(8) Abruña, H. D.; Bommarito, G. M.; Acevedo, D. The Study of Solid/Liquid Interfaces with X-ray Standing Waves. *Science* **1990**, *250*, 69−74.
(9) Gomez, R.; Yee, H. S.; Bommarito, G. M.; Feliu, J. M.; Abruña, H. D. Anion Effects and the Mechanism of Cu UPD on Pt(111): X-ray and Electrochemical Studies. *Surf. Sci.* **1995**, *335*, 101−109.
(10) Gordon, J. G.; Melroy, O. R.; Toney, M. F. Structure of Metal-Electrolyte Interfaces: Cu on Au(111), Water on Ag(111). *Electrochim. Acta* **1995**, *40*, 3−8.
(11) Finnefrock, A. C.; Ringland, K. L.; Brock, J. D.; Buller, L. J.; Abruña, H. D. Nucleation and Ordering of an Electrodeposited Two-Dimensional Crystal: Real-Time X-Ray Scattering and Electronic Measurements. *Phys. Rev. Lett.* **1998**, *81*, 3459−3462.
(12) Tadjeddine, A.; Guay, D.; Ladouceur, M.; Tourillon, G. Electronic and Structural Characterization of Underpotentially Deposited Submonolayers and Monolayer of Copper on Gold (111) Studied by In Situ X-Ray-Absorption Spectroscopy. *Phys. Rev. Lett.* **1991**, *66*, 2235−2238.
(13) Möller, F. A.; Magnussen, O. M.; Behm, R. *In situ* STM studies of Cu Underpotential Deposition on Au(100) in the Presence of Sulfate and Chloride Anions. *Phys. Rev. B* **1995**, *51*, 2484−2490.
(14) Manne, S.; Hansma, P. K.; Massie, J.; Elings, V. B.; Gewirth, A. A. Atomic-Resolution Electrochemistry with the Atomic Force Microscope: Copper Deposition on Gold. *Science* **1991**, *251*, 183−186.
(15) Hachiya, T.; Honbo, H.; Itaya, K. Detailed Underpotential Deposition of Copper on Gold(111) in Aqueous Solutions. *J. Elecrroanal. Chem.* **1991**, *315*, 275−291.
(16) Haiss, W.; Sass, J.-K. Quantitative Surface Stress Measurements on Au(111) Electrodes by Scanning Tunneling Microscopy. *Langmuir* **1996**, *12*, 4311−4313.
(17) Williamson, M.; Tromp, R.; Vereecken, P.; Hull, R.; Ross, F. Dynamic Microscopy of Nanoscale Cluster Growth at the Solid−Liquid Interface. *Nat. Mater.* **2003**, *2*, 532−536.
(18) Schneider, N. M.; Park, J. H.; Grogan, J. M.; Steingart, D. A.; Bau, H. H.; Ross, F. M. Nanoscale Evolution of Interface Morphology during Electrodeposition. *Nat. Commun.* **2017**, *8*, 2174.
(19) Tian, X.; Luo, J.; Nan, H.; Zou, H.; Chen, R.; Shu, T.; Li, X.; Li, Y.; Song, H.; Liao, S.; Adzic, R. R. Transition Metal Nitride Coated with Atomic Layers of Pt as a Low-Cost, Highly Stable Electrocatalyst for the Oxygen Reduction Reaction. *J. Am. Chem. Soc.* **2016**, *138*, 1575−1583.
(20) Xiong, Y.; Yang, Y.; DiSalvo, F. J.; Abruña, H. D. Pt-Decorated Composition-Tunable Pd−Fe@Pd/C Core−Shell Nanoparticles with Enhanced Electrocatalytic Activity toward the Oxygen Reduction Reaction. *J. Am. Chem. Soc.* **2018**, *140* (23), 7248−7255.
(21) Ghosh, T.; Vukmirovic, M. B.; DiSalvo, F. J.; Adzic, R. R. Intermetallics as Novel Supports for Pt Monolayer O_2 Reduction Electrocatalysts: Potential for Significantly Improving Properties. *J. Am. Chem. Soc.* **2010**, *132*, 906−907.
(22) Wang, J. X.; Inada, H.; Wu, L. J.; Zhu, Y. M.; Choi, Y. M.; Liu, P.; Zhou, W. P.; Adzic, R. R. Oxygen Reduction on Well-Defined Core-Shell Nanocatalysts: Particle Size, Facet, and Pt Shell Thickness Effects. *J. Am. Chem. Soc.* **2009**, *131* (47), 17298−17302.
(23) Zhang, J.; Vukmirovic, M.; Xu, Y.; Mavrikakis, M.; Adzic, R. R. Controlling the Catalytic of Platinum-Monolayer Electrocatalysts for Oxygen Reduction with Different Substrates. *Angew. Chem., Int. Ed.* **2005**, *44*, 2132−2135.
(24) Lima, F.; Zhang, J.; Shao, M.; Sasaki, K.; Vukmirovic, M.; Ticianelli, E.; Adzic, R. Catalytic Activity-d-Band Center Correlation for the O_2 Reduction Reaction on Platinum in Alkaline Solutions. *J. Phys. Chem. C* **2007**, *111*, 404−410.
(25) Sasaki, K.; Kuttiyiel, K. A.; Su, D.; Adzic, R. R. Platinum Monolayer on IrFe Core−Shell Nanoparticle Electrocatalysts for the Oxygen Reduction Reaction. *Electrocatalysis* **2011**, *2*, 134−140.
(26) Adzic, R. R.; Zhang, J.; Sasaki, K.; Vukmirovic, M. B.; Shao, M.; Wang, J. X.; Nilekar, A. U.; Mavrikakis, M.; Valerio, J. A.; Uribe, F. Platinum Monolayer Fuel Cell Electrocatalysts. *Top. Catal.* **2007**, *46*, 249−262.
(27) Yang, Y.; Xiong, Y.; Zeng, R.; Lu, X.; Krumov, M.; Huang, X.; Xu, W.; Wang, H.; DiSalvo, F. J.; Brock, J. D.; Muller, D. A.; Abruña, H. D. *Operando* Methods in Electrocatalysis. *ACS Catal.* **2021**, *11*, 1136−1178.
(28) Kondo, T.; Morita, J.; Hanaoka, K.; Takakusagi, S.; Tamura, K.; Takahasi, M.; Mizuki, J.; Uosaki, K. Structure of Au(111) and Au(100) Single-Crystal Electrode Surfaces at Various Potentials in Sulfuric Acid Solution Determined by In Situ Surface X-ray Scattering. *J. Phys. Chem. C* **2007**, *111*, 13197−13204.
(29) Holtz, M. E.; Yu, Y.; Gunceler, D.; Gao, J.; Sundararaman, R.; Schwarz, K. A.; Arias, T. A.; Abruña, H. D.; Muller, D. A. Nanoscale Imaging of Lithium Ion Distribution during *In Situ* Operation of Battery Electrode and Electrolyte. *Nano Lett.* **2014**, *14*, 1453−1459.
(30) Yang, Y.; Shao, Y.-T.; Lu, X.; Abruña, H. D.; Muller, D. A. Elucidating Cathodic Corrosion Mechanisms with *Operando* Electrochemical Liquid-Cell STEM in Multiple Dimensions. *Microsc. Microanal.* **2021**, *27*, 238−239.
(31) Emanuel, A.; Olander, D. R. Diffusion Coefficients of Copper Sulfate in Water and Water in n-Butyl Alcohol. *J. Chem. Eng. Data* **1963**, *8*, 31−32.
(32) Schwarzacher, W. Kinetic Roughening of Electrodeposited Films. *J. Phys.: Condens. Matter* **2004**, *16*, R859−R880.
(33) Tate, M. W.; Purohit, P.; Chamberlain, D.; Nguyen, K. X.; Hovden, R.; Chang, C. S.; Deb, P.; Turgut, E.; Heron, J. T.; Schlom, D. G.; Ralph, D.; Fuchs, G. D.; Shanks, K. S.; Philipp, H. T.; Muller, D. A.; Gruner, S. M. High Dynamic Range Pixel Array Detector for Scanning Transmission Electron Microscopy. *Microsc. Microanal.* **2016**, *22*, 237−249.
(34) Chen, Z.; Jiang, Y.; Shao, Y.-T.; Holtz, M. E.; Odstrcil, M.; Guizar-Sicairos, M.; Hanke, I.; Ganschow, S.; Schlom, D. G.; Muller, D. A. Electron Ptychorgraphy Achieves Atomic-Resolution Limits Set by Lattice Vibrations. *Science* **2021**, *372*, 826−831.
(35) Yang, Y.; Zeng, R.; Paik, H.; Kuo, D.-Y.; Schlom, D. G.; DiSalvo, F. J.; Muller, D. A.; Suntivich, J.; Abruña, H. D. Epitaxial Thin-Film Spinel Oxides as Oxygen Reduction Electrocatalysts in Alkaline Media. *Chem. Mater.* **2021**, *33*, 4006−4013.
(36) Eom, C. J.; Kuo, D.-K.; Adamo, C.; Moon, E. J.; May, S. J.; Crumlin, E. J.; Schlom, D. G.; Suntivich, J. Tailoring Manganese Oxide with Atomic Precision to Increase Surface Site Availability for Oxygen Reduction Catalysis. *Nat. Commun.* **2018**, *9*, 4034.
(37) Serra-Maia, R.; Kumar, P.; Meng, A. C.; Foucher, A. C.; Kang, Y.; Karki, K.; Jariwala, D.; Stach, E. A. Nanoscale Chemical and Structural Analysis during In Situ Scanning/Transmission Electron Microscopy in Liquids. *ACS Nano* **2021**, *15*, 10228−10240.
(38) Beermann, V.; Holtz, M. E.; Padgett, E.; de Araujo, J. F.; Muller, D. A.; Strasser, P. Real-Time Imaging of Activation and Degradation of Carbon Supported Octahedral Pt−Ni Alloy Fuel Cell Catalysts at the Nanoscale Using In Situ Electrochemical Liquid Cell STEM. *Energy. Envion. Sci.* **2019**, *12*, 2476−2485.
(39) Li, Y.; Kim, D.; Louisia, S.; Xie, C.; Kong, Q.; Yu, S.; Lin, T.; Aloni, S.; Fakra, S.; Yang, P. Electrochemically Scrambled Nanocrystals are Catalytically Active for CO_2-To-Multicarbons. *Proc. Natl. Acad. Sci. U. S. A.* **2020**, *117*, 9194−9201.
(40) Aran-Ais, R. M.; Rizo, R.; Grosse, P.; Algara-Siller, G.; Dembele, K.; Plodinec, M.; Lunkenbein, T.; Chee, S. W.; Cuenya, B. R. Imaging Electrochemically Synthesized Cu_2O Cubes and Their Morphological Evolution under Conditions Relevant to CO_2 Electroreduction. *Nat. Commun.* **2020**, *11*, 3489.
(41) Yang, Y. et al. Electrocatalysis in Alkaline Media and Alkaline Membrane-Based Energy Technologies. *Chem. Rev.* **2022**.

https://doi.org/10.1021/acsenergylett.2c00209
ACS Energy Lett. 2022, 7, 1292−1297